# Open Archive TOULOUSE Archive Ouverte (OATAO)

OATAO is an open access repository that collects the work of Toulouse researchers and makes it freely available over the web where possible.

Any correspondence concerning this service should be sent to the repository administrator: staff-oatao@listes-diff.inp-toulouse.fr

# A new numerical method for axial dispersion characterization in microreactors

Maxime Moreau, Nathalie Di Miceli Raimondi *, Nathalie Le Sauze, Christophe Gourdon, Michel Cabassud

*Laboratoire de Génie Chimique, Université de Toulouse, CNRS, INPT, UPS, 4 Allée Emile Monso, F-31432 Toulouse, France*

## HIGHLIGHTS

- An innovative numerical method for axial dispersion characterization is proposed.
- The method is validated thanks to a RTD experiment in a microchannel.
- The method is applied to rectangular millimetric wavy channels.
- The impact of the channel geometry on the axial dispersion coefficient is studied.

## ABSTRACT

Axial dispersion is a key phenomenon in reactor engineering that can affect yield and selectivity when reactions are carried out. Therefore its characterization is necessary for an adequate modelling of the reactor. The development of compact reactors to fit with process intensification expectations requires the use of characterization methods adapted to small-scale devices. An original method not-frequently used up to now for the estimation of axial dispersion coefficients is presented and applied to millimetric wavy channels. It is based on CFD simulations to calculate velocity and concentration fields from which axial dispersion coefficient can be estimated. This method is used to predict the impact of the wavy channel geometry and of the fluid velocity on axial dispersion in laminar flow regime. The investigated geometrical parameters are the hydraulic diameter (2–4 mm), the cross-sectional aspect ratio defined as the ratio between the channel width and its depth (0.25–1) and the internal curvature radius of the bends (2–3.4 mm). The range of Reynolds number considered is $Re$ = 70–1 600. Axial dispersion coefficient increases with velocity, values range from $2.8 \cdot 10^{-4}$ to $3.2 \cdot 10^{-3}$ m$^2 \cdot$s$^{-1}$. It appears that axial dispersion varies slightly in function of the channel hydraulic diameter. Square wavy channels generate less axial dispersion than rectangular wavy ones. Finally, axial dispersion coefficient increases with the internal curvature radius which shows the positive impact of sharp bends to reduce axial dispersion effect.

## 1. Introduction

At the core of chemical engineering, reactor design is fundamental to reach a goal of productivity. A rigorous management of the operating conditions (flow rate, temperature, pressure, etc.) is notably necessary to limit the production of by-products and to carry out the reaction safely (Nikačević et al., 2012). It requires the control of the different transfer mechanisms related to mixing, heat transfer and mass transfer in homogeneous or heterogeneous media. For that purpose, fine chemistry and pharmaceutical industries usually slow down the intrinsic kinetics (dilution, low temperature, fed-batch operation, etc.) so that the process is not limited by the kinetics of transport phenomena. In a concern of a greener chemistry, process intensification advocates since a few years the development of technologies which adapt themselves to the implemented chemistry and not the opposite (Van Gerven and Stankiewicz, 2009). The objective is to work under adequate operating conditions that ensure a safe process, limit the use of solvents and optimize energy consumption (notably by means of the reduction of operations that follow reaction such as separations and waste treatments). The intensification of the chemical reactors is often envisaged for the implementation of exothermic reactions, since a bad control of the temperature may degrade the production and even worse, cause serious damages due to thermal runaways. Today, numerous technologies of intensified reactors are available among which microreactors (Anxionnaz et al., 2008; Lutze et al., 2010). They offer an important exchange area compared to the vol-

\* Corresponding author.
 *E-mail address:* nathalie.raimondi@iut-tlse3.fr (N. Di Miceli Raimondi).

ume of the reactor for an enhancement of heat transfer. The reactive fluid circulates generally at moderate velocity to provide enough residence time for the reaction. So, due to the low size of the intensified devices and the low velocity of the fluids, flow regimes are often laminar in microreactors. Therefore, to ensure a fast contact between reactants, these technologies are commonly designed according to complex geometries in order to intensify mixing despite laminar flow. It results in particular hydrodynamic behaviours (Amador et al., 2008; Boskovic and Loebbecke, 2008; Moreau et al., 2015) that need to be characterized in order to detect possible flow defaults. Global hydrodynamic characterization of reactors also gives information about the global hydrodynamic behaviour of a device (from the plug flow to the perfectly stirred tank character) for an adequate modelling of the reactor (Levenspiel, 1999). The objective is then to obtain a reliable estimate of conversion rate and selectivity. Tubular reactors are generally modelled as plug flow reactors with axial dispersion. In a perfect plug flow, all the fluid elements have the same residence time. Axial dispersion reflects the heterogeneity of the residence times due to molecular diffusion, velocity profile, turbulence, dead zones and other flow defaults.

The dispersion model consists in a one-dimension equation resulting from the projection along the main direction of the flow of the general transport equation of a chemical species in an incompressible fluid (convection-diffusion equation). In steady state, for a reactant A, this model can be written as follows:

$$\langle u_z \rangle \frac{d\langle C_A \rangle}{dz} - D_{ax} \frac{d^2\langle C_A \rangle}{dz^2} - r_A = 0 \tag{1}$$

where $\langle u_z \rangle$ and $\langle C_A \rangle$ are respectively the velocity and the concentration of A averaged over the reactor cross-section, $D_{ax}$ is the axial dispersion coefficient, $r_A$ is the rate of reaction of A and $z$ is the coordinate along the main direction of the flow.

The present article describes and discusses classical methods to estimate axial dispersion coefficients in a device and focuses on an original method based on simulations. The method is then applied to characterize microreactors that consist of millimetric wavy channels of different cross-section shapes and dimensions. The objective is to evaluate the impact of the channel geometry on axial dispersion with an objective of process scale-up.

## 2. Methods for axial dispersion characterization

### 2.1. Models for axial dispersion coefficient estimation

Models exist to estimate axial dispersion coefficient in tubular reactor, according to the device geometry and the flow regime related to Reynolds number (Eq. (2)):

$$Re = \frac{\rho \langle u_z \rangle d_H}{\mu} \tag{2}$$

For laminar flow in tubular pipes ($Re < 2100$), Taylor (1953) and Aris (1956) established a relation between the axial dispersion coefficient, the molecular diffusion coefficient, the hydraulic diameter and the average velocity (Eq. (3)). Squires and Quake (2005) and Ajdari et al. (2006) proposed similar correlations for non-circular pipes.

$$D_{ax} = D_m + \frac{\langle u_z \rangle^2 d_H^2}{192 D_m} \tag{3}$$

However, this model is only applicable when the characteristic time of axial convection is very high compared to the characteristic time of tangential diffusion (i.e. a molecule entering the center of the pipe must have enough time to migrate to the wall by diffusion before leaving the pipe). This condition can be written in terms of Eq. (4) (Nagy et al., 2012).

$$\frac{L}{\langle u_z \rangle} > 0.04 \frac{d_H^2}{D_m} \tag{4}$$

Mathematical models can also be used in laminar flow using pure convective Residence Time Distribution theory (Wörner, 2010). These models are applicable for fully developed flows in

circular or rectangular channels with fluids characterized by very high Schmidt number ($Sc = \mu/(\rho D_m)$) so that dispersion by molecular diffusion can be neglected.

In turbulent regime ($Re > 3000$) and for straight circular pipes the relationship between the axial dispersion coefficient and Reynolds number is written as follows (Trambouze and Euzen, 2004):

$$\frac{D_{ax}}{\langle u_z \rangle d_H} = \frac{3 \cdot 10^7}{Re^{2.1}} + \frac{1.35}{Re^{0.125}} \tag{5}$$

These models are applicable to simple geometries with limited velocity ranges or very long lengths (see Eq. (4)) while microreactors consist generally in short complex channel patterns to enhance mixing and transfer performances despite laminar flow condition. Therefore, experiments or simulations are generally required to characterize axial dispersion in a particular reactor.

## 2.2. Experimental methods

Axial dispersion coefficient is mainly estimated from Residence Time Distribution (RTD) experiments. The protocol consists in the injection of a tracer into the main fluid. The injection may not disturb the flow nor modify the physicochemical properties of the main fluid. It is detected at the reactor input and output. The obtained inlet and outlet signals are then analyzed in order to calculate the mean residence time inside the reactor and the axial dispersion coefficient (Levenspiel, 1999). The choice of the tracer depends on the analysis method. The main methods for liquid phase tracing are given below:

- Radioactivity (Kolar et al., 1987; Blet et al., 2000; Lelinski et al., 2002; Borroto et al., 2003): the main advantage of radioactivity measurements are the good accuracy (high detection sensitivity) and the fast response time of the sensors. However, this method is not-frequently used in liquid phase tracing due to the price of radioactive tracers and the risk of contamination and irradiation. It is more common for gas phase RTD where other types of tracer are not soluble.
- Thermal tracing: despite the simplicity of this method and its low cost, it is rarely used because it is intrusive (temperature sensors in the flow). The response time is high (thermal inertia) and the signals are highly disturbed notably by thermal losses and conduction in materials.
- Conductivity detection (Sancho and Rao, 1992; Gutierrez et al., 2010; Mohammadi and Boodhoo, 2012): this method is widely used because it is easy to implement at moderate cost. However, limitations exist for application in micro-devices diagnosis: the intrusive character of the method, the size of the probes and their response time (generally a few seconds). However new devices are proposed in response to these limitations such as wire-mesh sensors (Elias and Rudolf von Rohr, 2016; Häfeli et al., 2013).
- Optical detection: although the material is expensive and fragile, optical detection (e.g. UV–vis spectrophotometry (Boskovic and Loebbecke, 2008; Adeosun and Lawal, 2009; Günther et al., 2004; Kurt et al., 2015), fluorescence techniques (Lohse et al., 2008)) is very often used in microreactors because the response time of the sensors is of some hundred milliseconds. Moreover, these methods can be non-intrusive as far as the detection zone is transparent.

Even though they are very commonly used, experimental RTD presents significant drawbacks notably for the characterization of microreactors, i.e. devices of small volumes:

- RTD can be sensitive to the injection method since it can locally disturb the flow rate and the pressure. To avoid this effect, for a Dirac-like injection, an injection loop prefilled with tracer should be preferred to a syringe injection. A step-like injection can also be carried out switching from the main fluid to the solution of tracer at the entrance of the reactor. However, both methods require to manipulate valves which can bring air bubbles in the fluid, leading to a disturbance of the signals.
- Processing of the signals is required to take into account the non-ideality of the entrance signal such as convolution-deconvolution technique (Adeosun and Lawal, 2009; Gutierrez et al., 2010) and the noise related to the analysis method. This processing often generates a loss of information, notably related to the signal trail. This leads to a global underestimation of the axial dispersion.
- The analyzed zone must be representative of the reactor cross-section. This can be problematic if the channel size is larger than the sensor diameter. The use of cross-shape measuring cells can also be considered. In such a cell the fluid flows in a channel with the exact dimension of the probes. However, it leads to supplementary volumes (cells and connectors) at the reactor inlet and outlet characterized by their own residence time and axial dispersion. These secondary volumes can be significant compared to the usual volume of a microreactor, leading to an unreliable estimation of the axial dispersion generated only by the reactor.

## 2.3. Numerical methods

Thanks to the recent advances in computational capabilities and in CFD softwares (solving algorithms, design and meshing of complex geometries), many studies deal with numerical RTD. Two main methods are used:

- Particle tracking (Castelain et al., 2000; Sahle-Demessie et al., 2003; Le Moullec et al., 2008; Bai et al., 2008; Aubin et al., 2009; Habchi et al., 2010): this method is based on the simulation of the transport of Lagrangian particles injected at the reactor inlet at a given time (pulse injection). The trajectory of the particles obeys the force balance. Their characteristics are chosen so that they perfectly follow the elements of fluids (very small diameter and same density as the main fluid). The disadvantage of this method is that the tracer is not submitted to molecular diffusion. With a no-slip boundary condition at the reactor walls, particles injected near the walls may leave the reactor after a very long time, notably in laminar flow (Castelain et al., 2000; Bai et al., 2008; Aubin et al., 2009). In real flow conditions, the tracer at the wall would have been tangentially transported towards the reactor core by molecular diffusion. The trapped particles tend to emphasize the trail in RTD curve, leading to an overestimation of axial dispersion coefficient. Therefore, the RTD curve is generally truncated (some particles are neglected): the value of the resulting axial dispersion coefficient depends on the percentage of particles neglected. This method is so consistent when molecular diffusion is negligible compared to the other sources of transport. It may not be the case in confined devices with small characteristic dimensions such as microreactors.
- Tracer transport (Le Moullec et al., 2008): the concentration field of a passive scalar (tracer concentration) is computed by solving the general transport equation. This method is less used than particle tracking since concentration transport introduces numerical diffusion. This artificial diffusion contributes to axial dispersion in simulated RTD, leading to an overestimation of axial dispersion coefficient. Numerical diffusion can be negligible compared to the other sources of dispersion but it generally requires very refined meshes and so highly time-consuming simulations.

As for experimental characterizations, numerical RTD require mathematical processing to identify the axial dispersion coefficient from the outlet signal. This post-processing can lead to significant loss of information. Talvy et al. (2007) proposed an alternative method based on the expression of the different contributions to axial dispersion as function of the velocity and the concentration fields (i.e. molecular diffusion, temporal dispersion and spatial dispersion) (Talvy et al., 2007; Le Moullec et al., 2008). Therefore, axial dispersion coefficient can be estimated from simulations solving the continuity equation, Navier-Stokes equations and the transport equation of a tracer. This method is described in details in the next section. Its main advantage is that it is not based on RTD and so does not require post-processing techniques (convolution-deconvolution techniques, particles counting, model fitting). However, like any numerical method, an adequate mesh should be used to obtain reliable simulations with negligible numerical diffusion.

## 3. Description of the numerical method

### 3.1. Mathematical formulation of the axial dispersion coefficient

The method proposed by Talvy et al. (2007) is based on the projection of the transport equation along the main direction of the flow (Talvy et al., 2007). The general transport equation without a source term (i.e. transport of an inert tracer) is expressed as:

$$\frac{\partial C}{\partial t} + \nabla \cdot (\vec{u}\, C) + \nabla \cdot (\vec{J}) = 0 \tag{6}$$

As illustrated in Fig. 1, the main direction of the flow is given by the z-direction. The integral over the section normal to the flow (i.e. channel cross-section) is applied to Eq. (6):

$$\frac{1}{S}\iint_S \frac{\partial C}{\partial t} ds + \frac{1}{S}\iint_S \nabla \cdot (\vec{u}\, C) ds + \frac{1}{S}\iint_S \nabla \cdot (\vec{J}) ds = 0 \tag{7}$$

The divergence operators can be divided into two contributions: the divergence in the plane normal to the flow ($\nabla_S \cdot$) and the derivative in the main flow direction ($\nabla_z \cdot (\vec{u}) = \partial u_z / \partial z$ considering a straight flow):

$$\frac{1}{S}\iint_S \frac{\partial C}{\partial t} ds + \frac{1}{S}\iint_S \nabla_S \cdot (\vec{u}\, C + \vec{J}) ds + \frac{1}{S}\iint_S \frac{\partial}{\partial z}(u_z C + J_z) ds = 0 \tag{8}$$

Then, the divergence theorem is applied. It postulates that the surface integral of the divergence of a vector is equal to the surface boundary integral of the vector flux ($\delta S$ is the boundary of the cross-section $S$ and $\vec{n}$ the normal vector to the boundary in the plan $S$):

$$\frac{1}{S}\iint_S \frac{\partial C}{\partial t} ds + \frac{1}{S}\int_{\delta S} (C\vec{u} \cdot \vec{n} + \vec{J} \cdot \vec{n}) dl + \frac{1}{S}\iint_S \frac{\partial}{\partial z}(u_z C + J_z) ds = 0 \tag{9}$$

The fluxes through the cross-section boundary, i.e. through the reactor walls, are null. Therefore the second term is null and Eq. (9) can be simplified:

$$\frac{1}{S}\iint_S \frac{\partial C}{\partial t} ds + \frac{1}{S}\iint_S \frac{\partial}{\partial z}(u_z C + J_z) ds = 0 \tag{10}$$

Considering a reactor with a constant cross-section, the surface integral and the derivate can be permuted:

$$\frac{\partial}{\partial t}\left(\frac{1}{S}\iint_S C\, ds\right) + \frac{\partial}{\partial z}\left(\frac{1}{S}\iint_S (u_z C + J_z) ds\right) = 0 \tag{11}$$

Eq. (12) is then obtained by assuming that the diffusive flux obeys Fick's law:

$$\frac{\partial}{\partial t}\left(\frac{1}{S}\iint_S C\, ds\right) + \frac{\partial}{\partial z}\left(\frac{1}{S}\iint_S \left(u_z C - D_m \frac{\partial C}{\partial z}\right) ds\right) = 0 \tag{12}$$

The surface integral is represented by a surface average operator (Eq. (13)).

$$\langle\rangle = \frac{1}{S}\iint_S ds \tag{13}$$

Therefore Eq. (12) can be written in terms of Eq. (14).

$$\frac{\partial \langle C\rangle}{\partial t} + \frac{\partial \langle u_z C\rangle}{\partial z} - \frac{\partial}{\partial z}\left\langle D_m \frac{\partial C}{\partial z}\right\rangle = 0 \tag{14}$$

Finally, the velocity and the concentration are expressed as the sum of an average value over the cross-section and a spatial fluctuation that represents the non-uniformity of velocity and concentration across the section:

$$u_z = \langle u_z\rangle + \tilde{u}_z \tag{15}$$

$$C = \langle C\rangle + \tilde{C} \tag{16}$$

Therefore the term $\langle u_z C\rangle$ in Eq. (14) can be expressed as follows:

$$\langle u_z C\rangle = \langle\langle u_z\rangle\langle C\rangle\rangle + \langle\langle u_z\rangle\tilde{C}\rangle + \langle\tilde{u}_z\langle C\rangle\rangle + \langle\tilde{u}_z\tilde{C}\rangle$$
$$= \langle u_z\rangle\langle C\rangle + \langle u_z\rangle\langle\tilde{C}\rangle + \langle\tilde{u}_z\rangle\langle C\rangle + \langle\tilde{u}_z\tilde{C}\rangle \tag{17}$$

The application of the average operator to Eqs. (15) and (16) gives $\langle\tilde{u}_z\rangle = 0$ and $\langle\tilde{C}\rangle = 0$. Therefore, Eq. (17) can be simplified:

$$\langle u_z C\rangle = \langle u_z\rangle\langle C\rangle + \langle\tilde{u}_z\tilde{C}\rangle \tag{18}$$

The last term of Eq. (18) represents a convective flux per unit area. It is classically modelled as the product between a diffusivity and a concentration gradient (Eq. (19)). In the present case, the term $\langle\tilde{u}_z\tilde{C}\rangle$ translates the tracer spreading due to the non-uniformity of the velocity across the reactor cross-section. Therefore the term of diffusivity $D_s$ is called the spatial dispersion coefficient.

$$\langle\tilde{u}_z\tilde{C}\rangle = -D_s \frac{\partial \langle C\rangle}{\partial z} \tag{19}$$

It leads to the following expression of Eq. (14):

$$\frac{\partial \langle C\rangle}{\partial t} + \frac{\partial \langle u_z\rangle\langle C\rangle}{\partial z} + \frac{\partial}{\partial z}\left(-D_s \frac{\partial \langle C\rangle}{\partial z}\right) - \frac{\partial}{\partial z}\left(D_m \frac{\partial \langle C\rangle}{\partial z}\right) = 0 \tag{20}$$
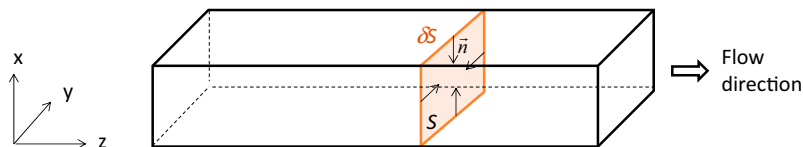


**Fig. 1.** Illustration of a reactor configuration.

Considering a constant cross-section and an incompressible fluid, the average velocity $\langle u_z \rangle$ is independent of the coordinate $z$. Therefore Eq. (20) can be written in terms of Eq. (21) (related to the unsteady general convection-dispersion equation without reaction):

$$\frac{\partial \langle C \rangle}{\partial t} + \langle u_z \rangle \frac{\partial \langle C \rangle}{\partial z} - \frac{\partial}{\partial z}\left(D_{ax}\frac{\partial \langle C \rangle}{\partial z}\right) = 0 \tag{21}$$

where $D_{ax}$ is the axial dispersion coefficient given by:

$$D_{ax} = D_m + D_s \tag{22}$$

It has to be noticed that stationary laminar flow is considered in this study. With unstationary flow (for instance in turbulent flow), a temporal dispersion coefficient also contributes to axial dispersion coefficient. It is obtained with an analogous mathematical process than the one described from Eqs. (7) to (22) applying a time average operator at Eq. (6), and by introducing temporal fluctuations in Eqs. (15) and (16) (Talvy et al., 2007; Le Moullec et al., 2008).

Eqs. (19) and (22) show that the axial dispersion coefficient can be predicted from the molecular diffusion coefficient and velocity and concentration fields obtained by CFD simulations:

$$D_{ax} = D_m + D_s = D_m - \frac{\langle \tilde{u}_z \tilde{C}\rangle}{\frac{\partial \langle C \rangle}{\partial z}} = D_m - \frac{\langle (u_z - \langle u_z \rangle)\cdot(C - \langle C\rangle)\rangle}{\frac{\partial \langle C\rangle}{\partial z}} \tag{23}$$

## 3.2. Computation method

The simulations were carried out according to two steps using the CFD software Comsol Multiphysics 4.3b: at first, the hydrodynamic behaviour of the system is computed in steady state. In a second step, the concentration field of a solute injected at the channel inlet is determined (transient simulation mode). The method assumes that (1) the main fluid and the tracer are perfectly miscible, (2) they are Newtonian and incompressible, (3) the physical properties of the main fluid are constant and not influenced by the presence of the tracer, (4) the solute concentration does not affect the flow structure.

The main fluid is water ($\rho$ = 1000 kg·m$^{-3}$, $\mu$ = 10$^{-3}$ Pa·s). Methylene blue is often used as a tracer in water using spectrophotometry technique for its detection. The value of its molecular diffusion coefficient in water is considered in the simulations as being $D_m = 6 \cdot 10^{-10}$ m$^2$·s$^{-1}$.

### 3.2.1. Hydrodynamics computation

The velocity field is governed by Navier-Stokes and continuity equations. Their expressions for an incompressible fluid flow in steady state are as follows:

$$\rho(\vec{u}\cdot\nabla)\vec{u} = \nabla\cdot(-P\mathbf{I} + \boldsymbol{\tau}) + \vec{F} \tag{24}$$

$$\rho\nabla\vec{u} = 0 \tag{25}$$

where $P$ is the pressure, $\mathbf{I}$ is the identity tensor, $\boldsymbol{\tau}$ is the viscous stress tensor and $\vec{F}$ represents the external forces (corresponding to the force of gravity in this work).

The boundary conditions are as follows:

- laminar velocity profile at the channel inlet;
- atmospheric pressure at the channel outlet and normal component of the stress null ($\boldsymbol{\tau}\cdot\vec{n} = 0$);
- no-slip velocity at the walls ($\vec{u} = 0$).

### 3.2.2. Tracer transport computation

The concentration field is obtained by solving the general mass transport equation for an incompressible fluid where the diffusive flux is given by Fick's law:

$$\frac{\partial C}{\partial t} + \nabla\cdot(-D_m\nabla C) + \vec{u}\cdot\nabla C = 0 \tag{26}$$

At initial time ($t = 0$), there is no tracer in the channel:$C = 0$. The boundary conditions are as follows:

- an injection function $C_i(t)$ is set at the channel inlet. Its expression is discussed in the next section;
- the conservation of the normal component of the flux at the channel outlet is assumed. In other terms the concentration gradient over the main direction of the flow is zero at the outlet. Regarding Eq. (23), this condition requires that the axial dispersion coefficient is calculated few cells before the outlet section;
- there is no flux through the walls. In other terms the concentration gradient over the direction normal to a wall is zero at this wall.

### 3.2.3. Tracer injection function

Unlike RTD experiments, the injection function of the tracer should not be a Dirac or a step. Indeed, regarding the expression of the axial dispersion coefficient (Eq. (23)), it is necessary to avoid the average concentration gradient to be zero at the section where $D_{ax}$ is calculated. Consequently, a linear function of time is used:

$$C_i(t) = 0\cdot 1t \tag{27}$$

Fig. 2 illustrates the impact of the injection function on the calculated axial dispersion coefficient. With a Dirac injection (Fig. 2 (a)), the value of $D_s$ is unstable with time while it reaches a plateau when Eq. (27) is applied (Fig. 2(b)). The time to reach the plateau is related to the time required for the tracer to be present in each of the nodes of the section where $D_{ax}$ is calculated. The value of the plateau is the one of interest since the continuous reactors are operated in steady-state.

### 3.3. Validation of the method in a circular straight capillary

#### 3.3.1. Comparison with Taylor and Aris model

The curves presented in Fig. 2 are obtained in a straight circular capillary of 2 mm inner diameter and 0.27 m length. The average velocity is 10$^{-4}$ m·s$^{-1}$. This simple geometry is used in a preliminary study to set-up and to validate the methodology. Indeed, such a geometry and operating conditions allows to satisfy Taylor and Aris condition given by Eq. (4):

$$\left[\frac{L}{\langle u_z\rangle} = 2700\right] > \left[0.04\frac{d_H^2}{D_m} = 267\right] \tag{28}$$

The geometry for the simulation consists in a 2D-axisymetric domain. The mesh is composed of uniform quadrilaterals with a size of 50 μm. Such a mesh allows to obtain a grid-independent solution. The axial dispersion coefficient predicted by the simulation is $D_{ax,simu}$ = 3.30 · 10$^{-7}$ m$^2$·s$^{-1}$. Taylor and Aris model expressed in terms of Eq. (3) gives $D_{ax,mod}$ = 3.48 · 10$^{-7}$ m$^2$·s$^{-1}$. It appears that both values are in a fairly good agreement, with a relative difference of 5.1%.

#### 3.3.2. Comparison with a RTD experiment

A RTD experiment is carried out in a PTFE tube of 2 mm inner diameter. A flow rate of 1.2 mL·h$^{-1}$ of water is delivered thanks to a neMESYS syringe pump. It gives an average velocity $\langle u_z\rangle$ = 10$^{-4}$ m·s$^{-1}$. RTD curves are obtained with a spectrophotometry technique using methylene blue as the tracer. Fig. 3 illustrates
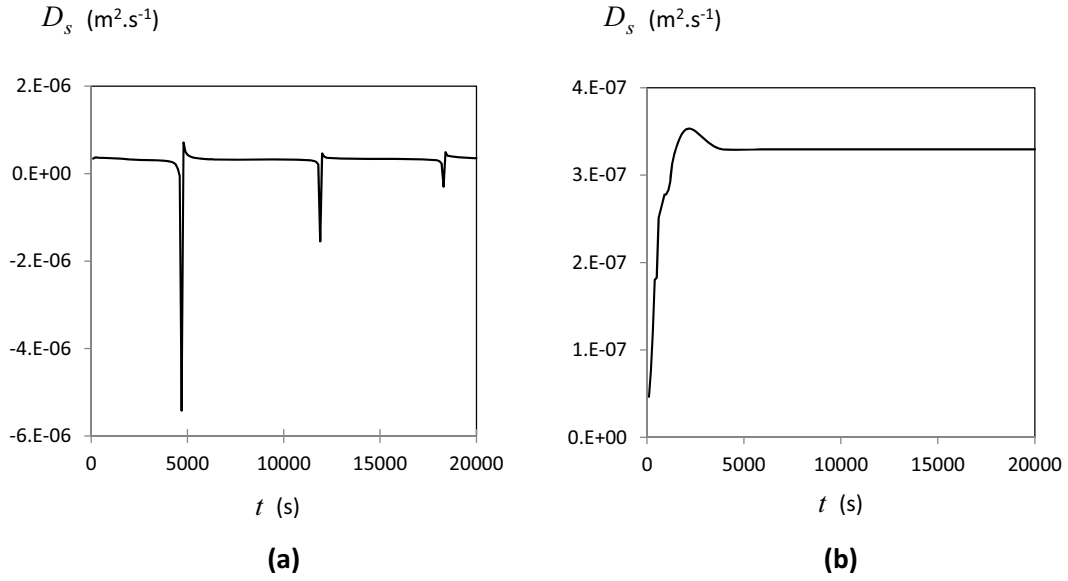
**Fig. 2.** Impact of the injection function of the tracer on the spatial dispersion coefficient: (a) with a Dirac function and (b) with Eq. (27). The simulations are carried out in a straight circular channel ($d_H$ = 2 mm, $L$ = 0.27 m, $\langle u_z \rangle = 10^{-4}$ m·s$^{-1}$).
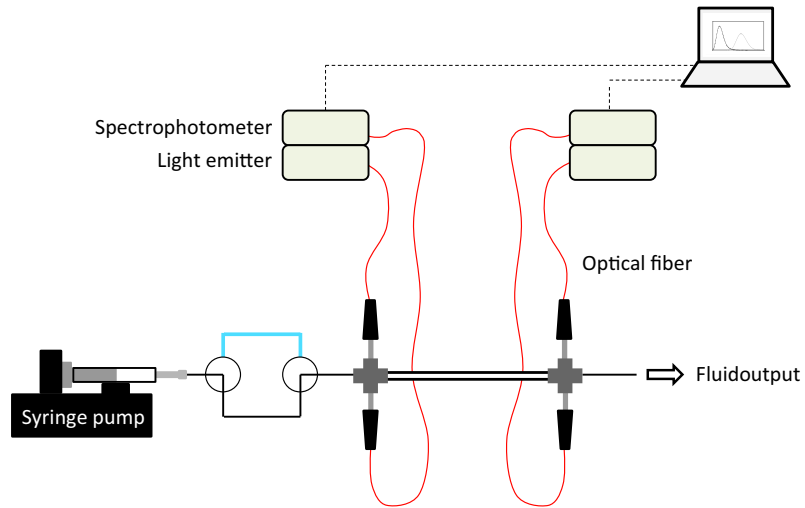


**Fig. 3.** Set-up for RTD experiments.

the experimental setup. Cross-shape Swagelok® connectors are used to position optical fibers at the inlet and outlet of the capillary. The length between the two set of fibers is 0.27 cm, corresponding to the length simulated. In a set of two optical fibers, one is connected to a light emitter, the other one to the spectrophotometer (AvaSpec-2048-USB2 Grating UA) which analysis the light received by the fiber to measure the absorbance of the fluid circulating through the fibers. The received signals are analyzed with the software Avasoft-Full. Thanks to a prior calibration of the system, the concentration of the tracer is obtained by integration of the absorbance function in a wavelength range of 630–670 nm. A loop prefilled with tracer is used at the fluid input to inject the tracer in the capillary. Two three-way valves allow to switch from the main tube to the tracer loop. The volume of the loop is small enough to obtain a Dirac-like injection function.

The RTD response to a Dirac-like injection is given by the distribution function $E(t)$ which is a normalized function of the average concentration over the analyzed cross-section (Fig. 4).

$$E(t) = \frac{\langle C \rangle (t)}{\int_0^\infty \langle C \rangle (t) dt} \tag{29}$$

With a perfect Dirac signal at the reactor inlet, the axial dispersion coefficient can be obtained by fitting with an analytical solution provided by a convection-dispersion model. In this work, in order to take into account the imperfection of the inlet signal, it is chosen to solve the 1D convection-dispersion equation in terms of distribution function (Eq. (30)) using the experimental inlet signal as boundary condition.

$$\frac{\partial E}{\partial t} + \langle u_z \rangle \frac{\partial E}{\partial z} - \frac{\partial}{\partial z}\left(D_{ax}\frac{\partial E}{\partial z}\right) = 0 \tag{30}$$

At initial time, there is no tracer in the channel: $E = 0$ at $t = 0$. The boundary conditions are as follows:

- experimental signal at the capillary inlet: $E(t) = E_{inlet,\exp}(t)$ at $z = 0$;
- conservation of the flux at the channel outlet: $\frac{\partial E}{\partial z} = 0$ at $z = L$.
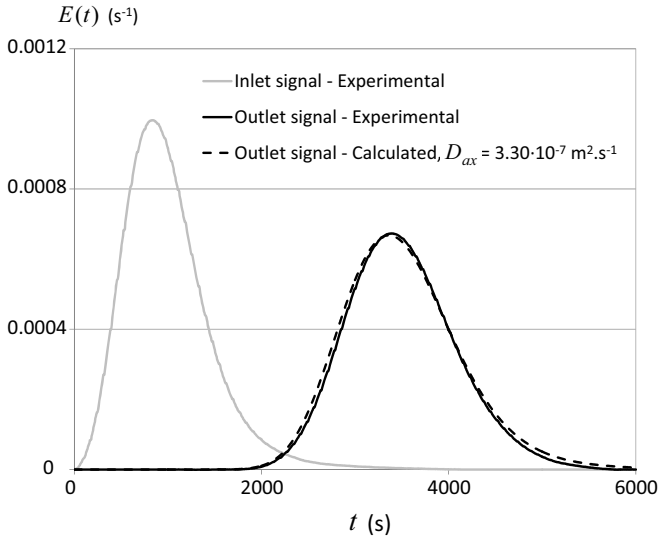
**Fig. 4.** Experimental RTD and calculated outlet signal using Eq. (30).

Eq. (30) is solved using Comsol Multiphysics 4.3b. $D_{ax}$ is set equal to the coefficient obtained with the numerical method, i.e. $D_{ax} = 3.30 \cdot 10^{-7}$ m$^2$·s$^{-1}$. As it can be seen in Fig. 4, such a value allows a very good prediction of the experimental outlet signal.

## 4. Application to millimetric wavy channels

### 4.1. Channel geometry

Wavy channels with different square and rectangular cross-sections have been considered in this study. Millimetric wavy channels are notably used in heat exchangers-reactors developed by the Laboratoire de Génie Chimique (LGC - Toulouse, France). These devices were built in different materials such as silicon carbide (built by Boostec company - France) or stainless steel (built by the Commissariat à l'énergie atomique et aux énergies alternatives, CEA - France). This pattern allows an enhancement of mixing, mass and heat transfer compared to straight channels with reasonable pressure drops (Anxionnaz-Minvielle et al., 2013). Indeed, despite laminar flow, the bends generate vortices, so-called Dean vortices (Dean, 1928), that promote species transport from the walls to the channel center. This device has been successfully used to carry out exothermic reactions (Elgue et al., 2012; Despènes et al., 2012; Di Miceli Raimondi et al., 2015).

The channel geometry consists in a periodic zigzag (Fig. 5). The straight length between two bends is $L_s$ = 10 mm. The bends are characterized by an angle of 90° and a curvature radius at the center of the channel of $R_c$ = 4 mm. The total developed length of the channel simulated is $L$ = 0.27 m which corresponds to 16 straight lengths and bends. Different cross-sections have been considered function of the channel width $w$ and depth $l$ as shown in Table 1.
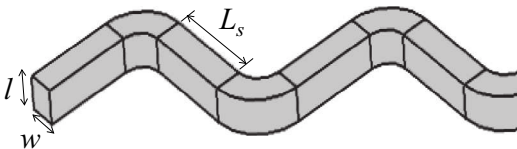


**Fig. 5.** Wavy channel geometry.

This allows to study the sensitivity of axial dispersion to the hydraulic diameter ($d_H = 2w \cdot l/(w + l)$) and to the aspect ratio of the section ($\alpha = w/l$; $\alpha = 1$ for a square section). For rectangular cross-sections, it has to be noted that deep channels have been considered in the present study because of the bend curvature. Deep channels are more flexible in terms of design compared to wide channels since lower curvature radii can be obtained, favoring the appearance of Dean vortices.

### 4.2. Structure and size of the mesh grid

For simple geometries, cartesian meshes should be used in simulations because they minimize numerical diffusion (Hirsch, 2007). In this work, because of the bends, a structured mesh adjusted at the curves or a tetrahedral mesh must be used. A structured mesh generates cells of very different sizes. Their volume decreases from the external side to the internal side of the bends. Very small cells may affect the convergence of the simulations and very small steps in time are so required to solve the equations, leading to highly time consuming simulations. Therefore, despite a loss in the simulation accuracy, a tetrahedral mesh is preferred to a structured mesh. However, it appeared that the axial dispersion coefficient estimated with Eq. (23) was fluctuating according to time with such an unstructured mesh. This fluctuation is mainly due to the need to interpolate the velocity and the concentration fields to calculate the terms averaged on the channel cross-section. Indeed the calculation nodes in the tetrahedral mesh do not fit with the channel cross-section. Therefore, a structured mesh (cubic mesh) is used locally around the section where the axial dispersion coefficient is calculated as illustrated in Fig. 6.

As it can be seen in Fig. 6, for each mesh, the size of the cells over a cross-section is uniform. Indeed, CFD simulations are generally carried out with refined meshes near the wall where the shear rate is maximal. Nevertheless, numerical diffusion increases with velocity: its impact is thus more significant in the zone where velocity is higher i.e. around the channel center and can be reduced by decreasing the mesh size. For these reasons, uniform meshes have been used.

The sensitivity of the axial dispersion coefficient to the size of both tetrahedral and cubic meshes was studied. As noted before, numerical diffusion has a major impact at the highest fluid velocity: the sensitivity study was carried out for the higher velocity condition for each channel geometry. The adequate sizes of the meshes (i.e. simulation results are mesh-independent) for the different studied cases are given in Table 2.

### 4.3. Results

Axial dispersion coefficients are estimated using the numerical methodology previously described. The ranges of average velocity simulated for each reactor geometry are given in Table 3, as well as the ranges of flow rate, Reynolds number and Dean number (Eq. (31)).

$$De = Re\sqrt{\frac{d_H}{R_c}} \tag{31}$$

The impact of the geometrical parameters (hydraulic diameter and aspect ratio of the cross-section) on axial dispersion is studied.

#### 4.3.1. Effect of hydraulic diameter

The geometries with a square cross-section are considered. Fig. 7 shows that axial dispersion coefficient increases with velocity, and so with flow rate, according to a linear trend. At constant average velocity, it appears that axial dispersion coefficient varies slightly in function of the hydraulic diameter (Fig. 7(a)). Axial

**Table 1**
Characteristics of the wavy channels.

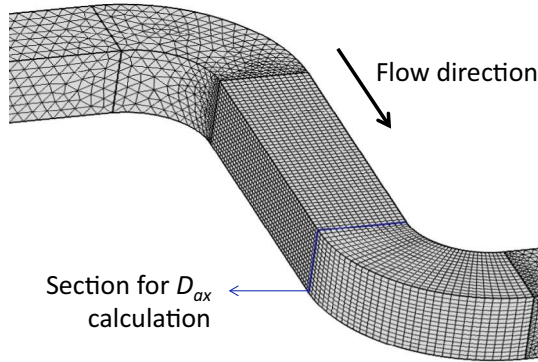| Geometry | $w$ (mm) | $l$ (mm) | $d_H$ (mm) | $\alpha$ | $S$ (mm$^2$) |
|---|---|---|---|---|---|
| (a) | 2 | 2 | 2 | 1 | 4 |
| (b) | 1.5 | 3 | 2 | 0.5 | 4.5 |
| (c) | 1.33 | 4 | 2 | 0.33 | 5.32 |
| (d) | 1.2 | 6 | 2 | 0.25 | 7.2 |
| (e) | 3 | 3 | 3 | 1 | 9 |
| (f) | 4 | 4 | 4 | 1 | 16 |



**Fig. 6.** Hybrid mesh grid used in the numerical method.

dispersion phenomenon significantly depends on the characteristic time to tangentially transport the tracer compared to the characteristic time to axially transport the tracer. At constant velocity in laminar flow, this last time is the same for the three geometries. However, time to tangentially transport the tracer is influenced by the hydraulic diameter: (i) in a negative way through the characteristic length of a tangential recirculation loop in a Dean vortex which increases with $d_h$ and (ii) in a positive way through Dean number which increases with $d_h$ implying more important tangential velocities. The weak influence of $d_h$ on $D_{ax}$ may be due to the competition between these two contradictory effects.

Since axial dispersion coefficient varies slightly in function of the hydraulic diameter at constant velocity, it obviously significantly decreases with the hydraulic diameter at constant flow rate due to the impact of this dimension on the cross-sectional area (Fig. 7(b)). These two figures illustrate the impact of different scale-up strategies on axial dispersion, for instance if the hydraulic diameter is increased to increase the flow rate (constant mean velocity) or to decrease the pressure drop (constant flow rate).

*4.3.2. Effect of cross-sectional aspect ratio*

The geometries with different cross-sectional aspect ratio for a constant hydraulic diameter of 2 mm are considered. It can be seen in Fig. 8 that axial dispersion coefficient increases with velocity, and so with flow rate. It appears that at constant average velocity, axial dispersion coefficient increases when the aspect ratio decreases with a sharp increase for $\alpha \leq 0.33$. Indeed, two sets of data can be distinguished: geometries (a) and (b) give similar results in terms of axial dispersion coefficient; the same observation can be made for geometries (c) and (d) but with significantly

higher values of axial dispersion coefficient than for the two other geometries. Aubin et al. (2009) compared axial dispersion coefficients in straight microchannels of square and rectangular cross-section. As in the present study, they observed a critical value of aspect ratio, approximately 0.3, from which a sharp decrease in the axial dispersion coefficient was observed. However, unlike in wavy channels, they showed that rectangular channels generate less axial dispersion than square channels. Wörner (2010) observed the same tendency. It implicitly means that the wavy configuration leads to opposite trends as regards axial dispersion in comparison with straight channels. These contradictory tendencies can be explained as follows. In laminar flow, at constant Reynolds number, axial dispersion effects can be reduced if the channel geometry allows to reduce the characteristic time to tangentially transport the tracer. In straight channel, this transport is ensured by molecular diffusion which is faster in rectangular channels than in square ones because the characteristic length of tangential diffusion is reduced (shortest dimension over the cross-section). Moreover, even when diffusive effects are negligible, Wörner (2010) argued that the ratio of the maximal velocity to the mean velocity is lower in rectangular channels than in square channels leading to a reduction of the axial dispersion of the tracer. Unlike straight channels, tangential transport by advection occurs in wavy channels due to Dean vortices. The ratio of the cross-section where tangential advection is efficient to the total cross-section is probably higher in square channels than in rectangular ones. A possible explanation lies in the increase of the wetted perimeter at constant hydraulic diameter (where velocity is zero) with the decrease of the aspect ratio.

*4.3.3. Modelling of axial dispersion*

In order to express the influence of the velocity, the hydraulic diameter and the cross-sectional aspect ratio on the axial dispersion coefficient, a correlation is proposed obtained from the simulation results presented in Fig. 7 and Fig. 8. It is expressed in terms of the dimensionless quantity $D_{ax}/(\langle u_z \rangle d_H)$ – which corresponds to the inverse of a Péclet number – as function of Reynolds number, Dean number and the cross-sectional aspect ratio:

$$\frac{D_{ax}}{\langle u_z \rangle d_H} = 4.5 \cdot Re^{1.38} De^{-1.68} \alpha^{-0.53} \tag{32}$$

Fig. 9 shows that Eq. (32) reasonably fits the simulation results, with an average relative error of 13.4% and a maximal relative error of 29%. The ranges of the parameters considered to establish the correlation are as follows: $d_H$ = 2–4 mm; $\alpha$ = 0.25–1; $Re$ = 70–1 600. The effect of the physicochemical properties of the fluid has not been investigated.

**Table 2**
Size of the meshes.

| Geometry | (a) | (b) | (c) | (d) | (e) | (f) |
|---|---|---|---|---|---|---|
| $\delta_{tetrahdral}$ (µm) | 150 | 200 | 100 | 200 | 75 | 200 |
| $\delta_{cubic}$ (µm) | 400 | 500 | 500 | 400 | 500 | 500 |

**Table 3**
Range of the simulated operating conditions.

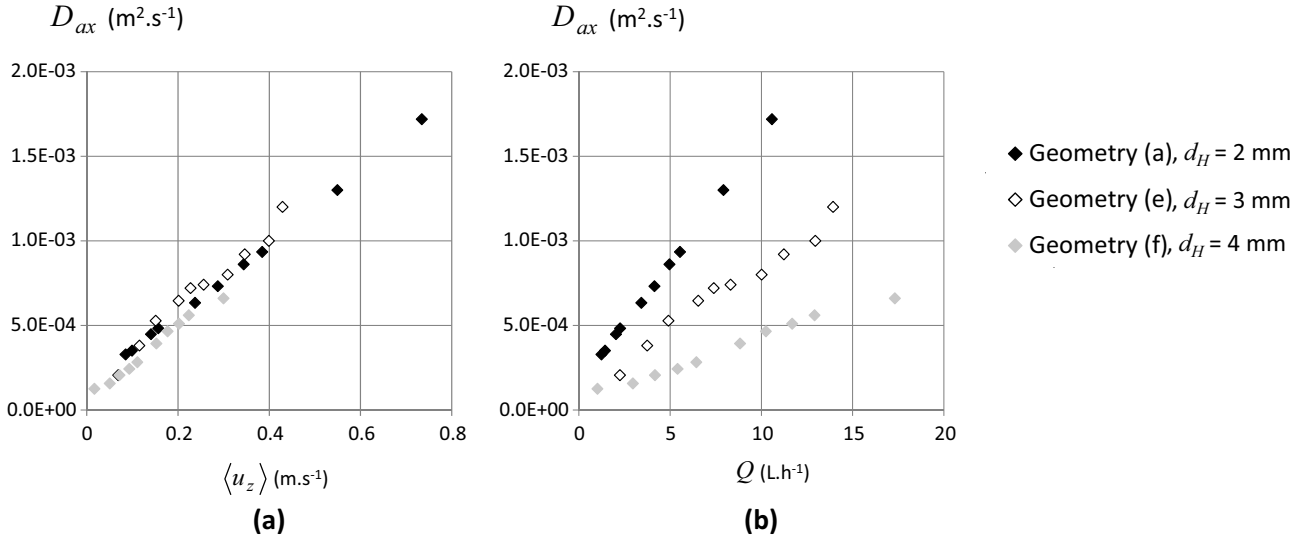| Geometry | $\langle u_z \rangle$ (m·s$^{-1}$) | $Q$ (L·h$^{-1}$) | $Re$ | $De$ |
|---|---|---|---|---|
| (a) | 0.086–0.74 | 1.2–10.6 | 172–1470 | 121–1040 |
| (b) | 0.050–0.88 | 0.8–14.2 | 100–1750 | 70–1238 |
| (c) | 0.064–0.36 | 1.2–7.0 | 128–727 | 90–514 |
| (d) | 0.061–0.80 | 1.6–20.7 | 122–1590 | 86–1128 |
| (e) | 0.070–0.43 | 2.3–13.9 | 209–1290 | 180–1118 |
| (f) | 0.018–0.30 | 1.0–17.3 | 71–1200 | 71–1203 |



**Fig. 7.** Axial dispersion coefficient vs (a) average velocity and (b) flow rate. Impact of the hydraulic diameter ($\alpha$ = 1).
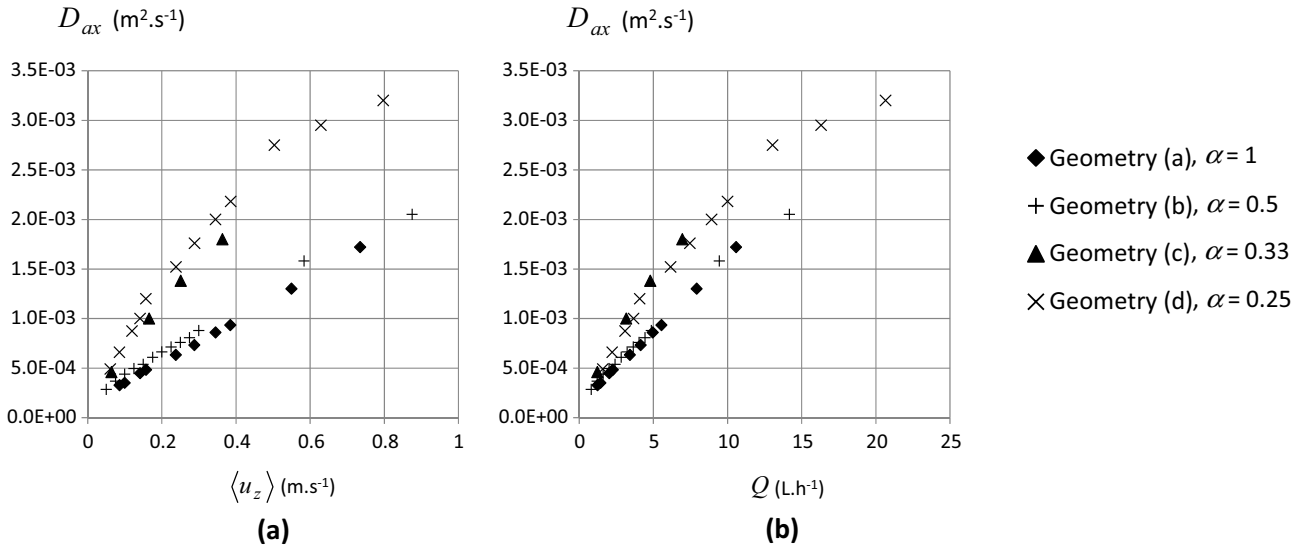


**Fig. 8.** Axial dispersion coefficient vs (a) average velocity and (b) flow rate. Impact of the aspect ratio of the channel cross-section ($d_H$ = 2 mm).

Eq. (32) can be compared to Eqs. (3) and (5) that give the dimensionless quantity $D_{ax}/(\langle u_z \rangle d_H)$ in a straight tube in laminar flow and turbulent flow respectively. In laminar flow, it can be seen that this quantity increases with the mean velocity. The opposite trend is observed in turbulent flow such as in the wavy channels despite laminar flow conditions. Indeed it is observed that $D_{ax}/(\langle u_z \rangle d_H)$ is proportional to $\langle u_z \rangle^{-0.3}$ in the present study.

### 4.3.4. Comparison with experimental results

RTD experiments have been carried out in a PMMA (poly(methyl methacrylate)) mock-up where a wavy channel corresponding to geometry (a) is engraved. The experimental method is analogous to the one described in Section 3.3.1. The mean velocity range studied is 0.086–0.39 m·s$^{-1}$. The channel length is the same than in the simulation work – $L$ = 0.27 m – resulting in

$D_{ax,mod}$ (m$^2$.s$^{-1}$)

- ◆ Geometry (a)
- + Geometry (b)
- ▲ Geometry (c)
- ✕ Geometry (d)
- ◇ Geometry (e)
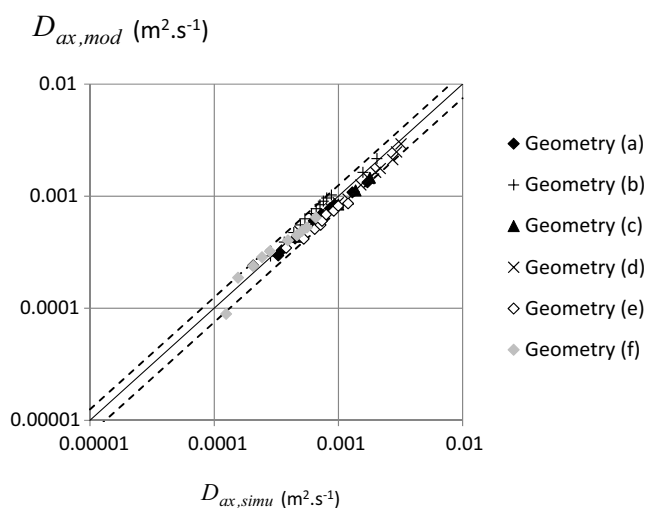- ◆ Geometry (f)

$D_{ax,simu}$ (m$^2$.s$^{-1}$)

**Fig. 9.** Comparison between axial dispersion coefficients obtained by simulations and calculated by the correlation given by Eq. (32). Dashed lines correspond to 25% of relative error.
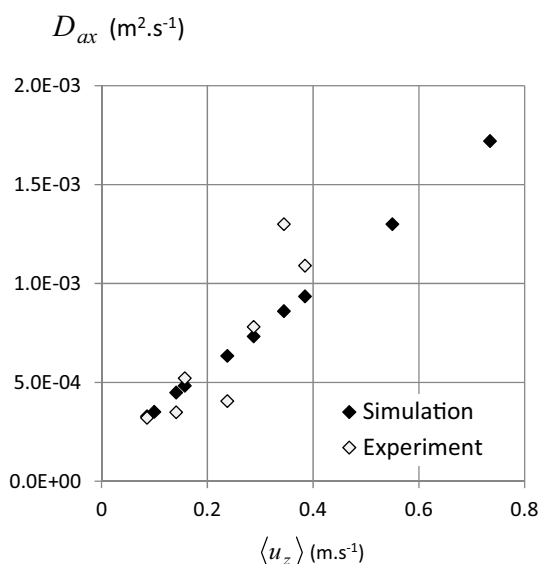


$D_{ax}$ (m$^2$.s$^{-1}$)

- ◆ Simulation
- ◇ Experiment

$\langle u_z \rangle$ (m.s$^{-1}$)

**Fig. 10.** Comparison between axial dispersion coefficients obtained by simulations and by RTD experiments in geometry (a).

residence times between 0.7 s and 3.1 s. Fig. 10 allows to compare the experimental results and those obtained thanks to the numerical method.

It can be observed that the numerical method allows to reproduce the global trend obtained with the experiments despite a significant uncertainty on the experimental points. This uncertainty is due to the perturbation of the flow at the injection of the tracer and the importance of the noise on the entrance and the outlet absorbance signals. This noise is related to the high frequency of acquisition (30 ms between each absorbance measurement) required to have a sufficient number of points on the RTD curves regarding the low residence times in the channel. These results illustrate the difficulty to accurately characterize axial dispersion in short residence time devices.

## 5. Conclusion

An original method for the characterization of axial dispersion in microreactors is presented. It is based on simulations using a CFD software. Comsol Multiphysics is used to solve continuity equation and Navier-Stokes equation to calculate the velocity field in the reactor, and the transport equation to predict the concentration field in tracer. These data allow the estimation of the axial dispersion coefficient considering an incompressible fluid and a reactor with a constant cross-section. In the present work, the method has been used under laminar flow regime and validated by comparison with an experimental result obtained from a RTD experiment in a circular straight capillary. This method can also be used in turbulent flow regime (Talvy et al., 2007) as long as an adequate turbulence model is used in the simulations.

The numerical method is applied to wavy millimetric channels with square and rectangular cross-section. Hydraulic diameters of 2–4 mm have been considered. Wavy channels are notably used in intensified compact reactors since the bends generate vortices that enhance mixing despite laminar flow and so heat and mass transfer. The study aims at investigating the impact of the cross-sectional aspect ratio of the channel and its hydraulic diameter on axial dispersion. It has been shown that square wavy channels generate less axial dispersion that rectangular ones, with a significant increase of axial dispersion coefficient at constant average velocity when the channel depth is more than three times higher than its width. Finally, in square channel, it appears that axial dispersion coefficient varies slightly in function of the hydraulic diameter at constant average velocity. These results have been expressed in terms of a correlation using dimensionless quantities that can be used then to predict the pertinent strategy to modify the operating conditions or the channel design in order to reduce axial dispersion phenomenon. However this correlation must be validated with other materials than water in order to study the influence of the fluid physicochemical properties on axial dispersion, and with geometries designed with various curvature radii and straight lengths between two bends to be more generic.

## References

Adeosun, J.T., Lawal, A., 2009. Numerical and experimental studies of mixing characteristics in a T-junction microchannel using residence-time distribution. Chem. Eng. Sci. 64, 2422–2432. http://dx.doi.org/10.1016/j.ces.2009.02.013.

Ajdari, A., Bontoux, N., Stone, H.A., 2006. Hydrodynamic dispersion in shallow microchannels: the effect of cross-sectional shape. Anal. Chem. 78, 387–392. http://dx.doi.org/10.1021/ac0508651.

Amador, C., Wenn, D., Shaw, J., Gavriilidis, A., Angeli, P., 2008. Design of a mesh microreactor for even flow distribution and narrow residence time distribution. Chem. Eng. J. 135, S259–S269. http://dx.doi.org/10.1016/j.cej.2007.07.021.

Anxionnaz-Minvielle, Z., Cabassud, M., Gourdon, C., Tochon, P., 2013. Influence of the meandering channel geometry on the thermo-hydraulic performances of an intensified heat exchanger/reactor. Chem. Eng. Process. Process Intensif. 73, 67–80. http://dx.doi.org/10.1016/j.cep.2013.06.012.

Anxionnaz, Z., Cabassud, M., Gourdon, C., Tochon, P., 2008. Heat exchanger/reactors (HEX reactors): concepts, technologies: state-of-the-art. Chem. Eng. Process. Process Intensif. 47, 2029–2050. http://dx.doi.org/10.1016/j.cep.2008.06.012.

Aris, R., 1956. On the dispersion of a solute in a fluid flowing through a tube. Proc. R. Soc. Lond. Math. Phys. Eng. Sci. 235, 67–77. http://dx.doi.org/10.1098/rspa.1956.0065.

Aubin, J., Prat, L., Xuereb, C., Gourdon, C., 2009. Effect of microchannel aspect ratio on residence time distributions and the axial dispersion coefficient. Chem. Eng. Process. Process Intensif. 48, 554–559. http://dx.doi.org/10.1016/j.cep.2008.08.004.

Bai, H., Stephenson, A., Jimenez, J., Jewell, D., Gillis, P., 2008. Modeling flow and residence time distribution in an industrial-scale reactor with a plunging jet inlet and optional agitation. Chem. Eng. Res. Des. 86, 1462–1476. http://dx.doi.org/10.1016/j.cherd.2008.08.012.

Blet, V., Berne, P., Legoupil, S., Vitart, X., 2000. Radioactive tracing as aid for diagnosing chemical reactors. Oil Gas Sci. Technol. 55, 171–183.

Borroto, J.I., Domínguez, J., Griffith, J., Fick, M., Leclerc, J.P., 2003. Technetium-99m as a tracer for the liquid RTD measurement in opaque anaerobic digester: application in a sugar wastewater treatment plant. Chem. Eng. Process. Process Intensif. 42, 857–865. http://dx.doi.org/10.1016/S0255-2701(02)00109-5.

Boskovic, D., Loebbecke, S., 2008. Modelling of the residence time distribution in micromixers. Chem. Eng. J. 135, S138–S146. http://dx.doi.org/10.1016/j.cej.2007.07.058.

Castelain, C., Berger, D., Legentilhomme, P., Mokrani, A., Peerhossaini, H., 2000. Experimental and numerical characterisation of mixing in a steady spatially chaotic flow by means of residence time distribution measurements. Int. J. Heat Mass Transf. 43, 3687–3700. http://dx.doi.org/10.1016/S0017-9310(99)00363-4.

Dean, W.R., 1928. Fluid motion in a curved channel. Proc. R. Soc. Lond. Math. Phys. Eng. Sci. 121, 402–420. http://dx.doi.org/10.1098/rspa.1928.0205.

Despènes, L., Elgue, S., Gourdon, C., Cabassud, M., 2012. Impact of the material on the thermal behaviour of heat exchangers-reactors. Chem. Eng. Process. Process Intensif. 52, 102–111. http://dx.doi.org/10.1016/j.cep.2011.11.005.

Di Miceli Raimondi, N., Olivier-Maget, N., Gabas, N., Cabassud, M., Gourdon, C., 2015. Safety enhancement by transposition of the nitration of toluene from semi-batch reactor to continuous intensified heat exchanger reactor. Chem. Eng. Res. Des. 94, 182–193. http://dx.doi.org/10.1016/j.cherd.2014.07.029.

Elgue, S., Conté, A., Gourdon, C., Bastard, Y., 2012. Direct fluorination. Chem. Today, 30.

Elias, Y., Rudolf von Rohr, P., 2016. Axial dispersion, pressure drop and mass transfer comparison of small-scale structured reaction devices for hydrogenations. Chem. Eng. Process. Process Intensif. 106, 1–12. http://dx.doi.org/10.1016/j.cep.2015.11.017.

Günther, M., Schneider, S., Wagner, J., Gorges, R., Henkel, T., Kielpinski, M., Albert, J., Bierbaum, R., Köhler, J.M., 2004. Characterisation of residence time and residence time distribution in chip reactors with modular arrangements by integrated optical detection. Chem. Eng. J. 101, 373–378. http://dx.doi.org/10.1016/j.cej.2003.10.019.

Gutierrez, C.G.C.C., Dias, E.F.T.S., Gut, J.A.W., 2010. Residence time distribution in holding tubes using generalized convection model and numerical convolution for non-ideal tracer detection. J. Food Eng. 98, 248–256. http://dx.doi.org/10.1016/j.jfoodeng.2010.01.004.

Habchi, C., Lemenand, T., Della Valle, D., Peerhossaini, H., 2010. Turbulent mixing and residence time distribution in novel multifunctional heat exchangers–reactors. Chem. Eng. Process. Process Intensif. 49, 1066–1075. http://dx.doi.org/10.1016/j.cep.2010.08.007.

Häfeli, R., Hutter, C., Damsohn, M., Prasser, H.-M., Rudolf von Rohr, P., 2013. Dispersion in fully developed flow through regular porous structures: experiments with wire-mesh sensors. Chem. Eng. Process. Process Intensif. 69, 104–111. http://dx.doi.org/10.1016/j.cep.2013.03.006.

Hirsch, C., 2007. Chapter 6 - structured and unstructured grid properties. In: Hirsch, C. (Ed.), Numerical Computation of Internal and External Flows. second ed. Butterworth-Heinemann, Oxford, pp. 249–277.

Kolar, Z., Thyn, J., Martens, W., Boelens, G., Korving, A., 1987. The measurement of gas residence time distribution in a pressurized fluidized-bed combustor using41Ar as radiotracer. Int. J. Rad. Appl. Instrum. 38, 117–122. http://dx.doi.org/10.1016/0883-2889(87)90006-2.

Kurt, S.K., Gelhausen, M.G., Kockmann, N., 2015. Axial dispersion and heat transfer in a milli/microstructured coiled flow inverter for narrow residence time distribution at laminar flow. Chem. Eng. Technol. 38, 1122–1130. http://dx.doi.org/10.1002/ceat.201400515.

Lelinski, D., Allen, J., Redden, L., Weber, A., 2002. Analysis of the residence time distribution in large flotation machines. Miner. Eng. 15, 499–505. http://dx.doi.org/10.1016/S0892-6875(02)00070-5.

Le Moullec, Y., Potier, O., Gentric, C., Leclerc, J.P., 2008. Flow field and residence time distribution simulation of a cross-flow gas–liquid wastewater treatment reactor using CFD. Chem. Eng. Sci. 63, 2436–2449. http://dx.doi.org/10.1016/j.ces.2008.01.029.

Levenspiel, O., 1999. Chemical Reaction Engineering. Wiley, New York.

Lohse, S., Kohnen, B.T., Janasek, D., Dittrich, P.S., Franzke, J., Agar, D.W., 2008. A novel method for determining residence time distribution in intricately structured microreactors. Lab Chip 8, 431. http://dx.doi.org/10.1039/b714190d.

Lutze, P., Gani, R., Woodley, J.M., 2010. Process intensification: a perspective on process synthesis. Chem. Eng. Process. Process Intensif. 49, 547–558. http://dx.doi.org/10.1016/j.cep.2010.05.002.

Mohammadi, S., Boodhoo, K.V.K., 2012. Online conductivity measurement of residence time distribution of thin film flow in the spinning disc reactor. Chem. Eng. J. 207–208, 885–894. http://dx.doi.org/10.1016/j.cej.2012.07.120.

Moreau, M., Di Miceli Raimondi, N., Le Sauze, N., Cabassud, M., Gourdon, C., 2015. Pressure drop and axial dispersion in industrial millistructured heat exchange reactors. Chem. Eng. Process. Process Intensif. 95, 54–62. http://dx.doi.org/10.1016/j.cep.2015.05.009.

Nagy, K.D., Shen, B., Jamison, T.F., Jensen, K.F., 2012. Mixing and dispersion in small-scale flow systems. Org. Process Res. Dev. 16, 976–981. http://dx.doi.org/10.1021/op200349f.

Nikačević, N.M., Huesman, A.E.M., Van den Hof, P.M.J., Stankiewicz, A.I., 2012. Opportunities and challenges for process control in process intensification. Chem. Eng. Process. Process Intensif. 52, 1–15. http://dx.doi.org/10.1016/j.cep.2011.11.006.

Sahle-Demessie, E., Bekele, S., Pillai, U.R., 2003. Residence time distribution of fluids in stirred annular photoreactor. Catal. Today 88, 61–72. http://dx.doi.org/10.1016/j.cattod.2003.08.009.

Sancho, M.F., Rao, M.A., 1992. Residence time distribution in a holding tube. J. Food Eng. 15, 1–19. http://dx.doi.org/10.1016/0260-8774(92)90037-7.

Squires, T.M., Quake, S.R., 2005. Microfluidics: fluid physics at the nanoliter scale. Rev. Mod. Phys. 77, 977.

Talvy, S., Cockx, A., Liné, A., 2007. Modeling hydrodynamics of gas–liquid airlift reactor. AIChE J. 53, 335–353. http://dx.doi.org/10.1002/aic.11078.

Taylor, G., 1953. Dispersion of soluble matter in solvent flowing slowly through a tube. Proc. R. Soc. Lond. Math. Phys. Eng. Sci. 219, 186–203. http://dx.doi.org/10.1098/rspa.1953.0139.

Trambouze, P., Euzen, J.-P., 2004. Chemical Reactors: From Design to Operation. Institut français du pétrole publications, Editions Technip, Paris.

Van Gerven, T., Stankiewicz, A., 2009. Structure, energy, synergy, time - the fundamentals of process intensification. Ind. Eng. Chem. Res. 48, 2465–2474. http://dx.doi.org/10.1021/ie801501y.

Wörner, M., 2010. Approximate residence time distribution of fully develop laminar flow in a straight rectangular channel. Chem. Eng. Sci. 65, 3499–3507. http://dx.doi.org/10.1016/j.ces.2010.02.047.